Desalination and Water Treatment
www.deswater.com
doi: 10.1080/19443994.2014.887034

54 (2015) 450–463
April

Taylor & Francis
Taylor & Francis Group

Polyaniline/basic oxygen furnace slag nanocomposite as a viable adsorbent for the sorption of fluoride from aqueous medium: equilibrium, thermodynamic and kinetic study

Mahamudur Islam[a,*], Mu Naushad[b], Rajkishore Patel[c]

[a]*Department of Chemistry, Purushottam Institute of Engineering & Technology, Purushottam Vihar, 10th km, Highway – 10, Mandiakudar, Kansbahal, Rourkela 770 034, Odisha, India*
Tel. +91 88952 70088; email: mahamudur.islam@gmail.com
[b]*Department of Chemistry, College of Science, Building # 5, King Saud University, Riyadh, Saudi Arabia*
[c]*Department of Chemistry, National Institute of Technology, Rourkela 769 008, Odisha, India*

Received 22 March 2013; Accepted 4 January 2014

ABSTRACT

The objective of the present research was to synthesize and characterize polyaniline/BOF slag nanocomposite and to evaluate its fluoride removal efficiency. The surface structure of the nanocomposite was investigated by means of XRD, TGA/DSC, SEM, and BET surface area analysis. In addition, adsorption mechanisms were investigated by conducting batch and making a comparative XRD analysis of fresh and exhausted nanocomposite. SEM micrographs were obtained to study the morphology of the nanocomposite. Batch experiments were performed to investigate effects of various experimental parameters such as contact time, initial fluoride concentration, temperature, pH, and the presence of competing anions. The adsorption data better fitted Langmuir adsorption isotherm. The maximum adsorption capacity calculated from Langmuir isotherm model was up to 9.143 mg/g (at 45˚C). Thermodynamic study indicated an endothermic nature of adsorption and a spontaneous and favorable process. The optimum pH for fluoride removal was between 6 and 10. The fluoride adsorption was impeded by the presence of phosphate, followed by bicarbonate, carbonate, sulfate, chloride, and nitrate. The fluoride removal was probably due to chemisorption, precipitation, and surface chemical reaction with CaO present in the basic oxygen furnace slag and through the replacement of doped ionizable chloride ions present in polyaniline.

Keywords: Polyaniline; Fluoride; Isotherms; Thermodynamic parameters; Basic oxygen furnace slag

1. Introduction

The prolonged intake of high concentrations of fluoride (more than 1.5 mg/L) in drinking water causes serious health problems. The physiological effects of fluoride ingestion on human health have been extensively studied. Fluoride is known to have both beneficial and detrimental effects on human health. The World Health Organization has set a guidance value of 1.5 mg/L for fluoride in drinking water [1]. A small amount of the principal mineral

---

*Corresponding author.

constituent, $Ca_5(PO_4)_3F$, can strengthen human teeth (specifically the enamel) and bones. However, prolonged exposure to high level of fluoride will lead to permanent bone/joint deformations and dental/skeletal fluorosis [2,3]. Also it leads to the irregular formation of collagen, which serves as a major structural component of skin, ligaments, tendons, muscles, cartilage, bones, and teeth. Most evidence indicates that fluoride can interfere with DNA synthesis [4]. The high concentrations of fluoride can also interfere with carbohydrates, lipids, proteins, vitamins, and mineral metabolism. Fluoride has several mechanisms of toxicity. Ingested fluoride initially acts locally on the intestinal mucosa. It can form hydrofluoric acid in the stomach, which leads to gastro-intestinal irritation or corrosive effects. Following ingestion, the gastro-intestinal tract is the earliest and most commonly affected organ system. Once absorbed, fluoride binds calcium ions and may lead to hypocalcaemia. Fluoride has direct cytotoxic effects and interferes with a number of enzyme systems; it disrupts oxidative phosphorylation, glycolysis, coagulation, and neurotransmission.

Fluoride in water derives mainly from dissolution of natural minerals in the rocks and soils with which water interacts. High fluoride concentrations can be built up in ground waters, which have long residence times in the host aquifers. In affected areas, the fluoride content of soils varies from less than 20 mg/L to an occasionally high level of 3,000 mg/L [5]. Fluoride is present in soil and rock formations in the form of fluorapatite, fluorspar, amphiboles, and micas [6,7]. Fluoride disperses to the environment through water, food, drugs, cosmetics, and several engineering process such as semiconductor manufacturing, coal power plants, glass and ceramic production, uranium refinement, electroplating, rubber, fertilizer manufacturing, and natural sources [8,9]. Fluoride is found in many common household products, including toothpaste (e.g. sodium monofluorophosphate), vitamins, dietary supplements (e.g. sodium fluoride), glass-etching or chrome-cleaning agents (e.g. ammonium bifluoride), insecticides, and rodenticides (e.g. sodium fluoride). Historically, most cases of fluoride toxicity have followed accidental ingestion of insecticides or rodenticides. The earliest problems associated with toxic wastes involved those businesses manufacturing aluminum with the resulting wastes usually being sodium fluoride.

There are several defluoridation techniques, which can be categorized into the following main categories namely precipitation, membrane processes, and ion exchange/adsorption onto various adsorbents. Various treatment technologies based on precipitation [3], ion exchange [10,11], adsorption [12,13], membrane process, such as reverse osmosis [14,15], nanofiltration [16], donnan dialysis [17], electrodialysis [18,19], and electrochemical technology, including electrocoagulation, electroflotation, and electrochemical oxidation [20], have been proposed for removal of fluoride from water. Some researchers [21,22] have demonstrated that electrocoagulation using aluminum anodes is effective in defluoridation. The combined electrocoagulation and electroflotation process is successfully applied in treating wastewater containing fluoride by Shen et al. [23]. Most methods for removing fluoride have drawbacks, including high initial cost, lack of selectivity, low removal capacity, and difficulty in operation or regeneration. Therefore, removal through adsorption is most promising in terms of cost of the medium, running cost, ease of operation, adsorption capacity, potential for reuse, number of useful cycles, and the possibility of regeneration [24]. Adsorption process involves the passage of the water through a contact bed where fluoride is removed by ion exchange, surface chemical reaction, or physical adsorption.

Since, adsorption was found to be one of the preferred methods for the remediation of fluoride, over the years considerable attention has been devoted to the development of better adsorbents. Defluoridation by adsorption process is the cheapest, simplest, and easy to implement for a developing country like India [25]. Materials like coconut shell carbon [26], activated carbon [27], activated alumina [28], bone char [29], ion exchange resins [30], zeolites [31], manganese dioxide-coated activated alumina [32], hydrous alumina [33] and polypyrrole [34] have been used as adsorbents. Most of these media show low capacity and moreover the time-scale for transferring an adsorbing species in the internal matrix of the adsorbent (diffusion time) is relatively large. To overcome this limitation, extensive research has been focused on advance techniques in material design.

Since the discovery of conducting polymers three decades ago, a large volume of research work has been performed associated with the physics and chemistry of conducting polymers. Among the family of conducting polymers, polyaniline is one of the most useful since it is air and moisture stable in both its doped, conducting form and in its dedoped, insulating form. Polyaniline is also unique among conducting polymers because it has a very simple acid/base doping/dedoping chemistry. It has a great variety of potential applications including anticorrosive coatings, batteries, sensors, separation membranes, antistatic coatings, and adsorbents. The ion exchange capacities of conducting polymers were well understood and it was found to depend on the polymerization conditions, the type and size of the dopants incorporated during the polymerization process as well as on the ions present in the electrolyte solution, the polymer thickness and aging of the polymer. Recently, conducting polymer/inorganic hybrid composites have attracted more attention, because they combine the merits of conducting polymers and inorganic materials. They have unusual hybrid mechanical, thermal, physical and chemical properties. They also have large surface area, which makes the polymer composite as good adsorbent as the pure polymer and inorganic host.

In recent years, the management of basic oxygen furnace (BOF) slag has become a significant issue due to the enormous quantities generated and the associated disposal costs and constraints. BOF slag is heterogeneous oxide materials which are compounded by some main oxides such as CaO, Fe_2O_3, SiO_2, Al_2O_3, and MgO. The heterogeneity of the BOF slag surface stems from two sources, namely geometrical and chemical. The geometrical heterogeneity (porosity) is the result of differences in the size and shape of pores, as well as pits, vacancies, and steps. Chemical heterogeneity is associated with different functional groups at a surface, and with various surface contaminants. Both the chemical and geometrical heterogeneities contribute to the unique adsorptive properties of BOF slag [35]. In other instances, conjunctive evidences from literature have also shown that BOF slag can help remove fluoride in wastewater. This is attributed to the abundant calcium and aluminum ions in the treated BOF slag, which enhance the processes of adsorption and chemical precipitation that help to remove fluoride from wastewater [36].

In the present research, polyaniline/BOF slag nanocomposite was synthesized for the removal of fluoride from aqueous solution. However, an in-depth understanding of the mechanisms and characteristics of fluoride adsorption by the polyaniline/BOF slag nanocomposite is crucial to its effective utilization as an adsorbent material. Therefore, the objective of this research was to synthesize, characterize, and to study the feasibility of using polyaniline/BOF slag nanocomposite as an adsorbent for the removal of fluoride from aqueous solution. The surface structure of the material was investigated by means of XRD, TGA/DSC, SEM, BET surface area analysis, etc. The adsorption characteristics of polyaniline/BOF slag nanocomposite for fluoride removal from aqueous solutions were evaluated in batch adsorption experiments.

2. Materials and methods

2.1. Chemicals used

Anilinium hydrochloride and ammonium peroxydisulfate (oxidant) used were of analytical grade and were purchased from Merck. All solvents used were of analytical grade and were freshly distilled before use. The standard fluoride solutions with different concentrations were prepared by serial dilution of NaF stock solution (1,000 mg/L). The measuring cylinder, volumetric flask, conical flask, and other glassware used were of Borosil.

2.2. Collection and processing of BOF slag

BOF slag used in the present research was generated from the local iron and steel plant with 2 years setting time. These samples were ground to powder by ball mill. The powdered sample was sieved to < 150 μm and then the BOF slag was thermally treated at a temperature of 1,000 °C for 24 h before the polyaniline/BOF slag nanocomposite was synthesized.

2.3. Preparation of polyaniline/BOF slag nanocomposite

Polyaniline/BOF slag nanocomposite was synthesized using anilinium hydrochloride, ammonium peroxydisulfate and treated BOF slag. 2.59 g of anilinium hydrochloride and 2 g of treated BOF (Thermally treated at a temperature of 1,000 °C for 24 h) slag were dispersed in 50 mL of distilled water in a volumetric flask. 5.71 g of ammonium peroxydisulfate was dissolved in 50 mL of distilled water. Both solutions/suspensions were kept for 1 h at room temperature (25 °C), then mixed in a beaker and was allowed to react for 24 h at 25 °C in the presence of ultrasonication. Next day, the resultant colloidal dispersion of polyaniline/BOF slag nanocomposite was ultracentrifuged at 40,000 rpm for 30 min, and separated as deep green sediments. The sediments were rinsed several times with distilled water and finally with acetone. Finally, the product was dried in an oven at 60 °C for 24 h.

2.4. Characterization of polyaniline/BOF slag nanocomposite

Elemental, physical, and chemical analyses of the BOF slag were carried out using inductively coupled plasma-atomic emission spectrometer (ICP-AES, IRIS Advantage). Scanning electron micrographs of the sample were obtained by JEOL JSM—6480LV scanning electron microscope. Energy dispersive X-ray spectroscopy (EDS or EDX) is an analytical technique which utilizes X-rays that are emitted from the specimen when bombarded by the electron beam. This technique was used for the elemental analysis. BET (Brunauer Emmett Teller) surface area of the sample was measured at liquid nitrogen temperature using BET surface area analyzer (QUANTACHROME Autosorb I). Powder XRD (X-ray Diffraction) of the material was obtained using PHILLIPS X′PERT X-ray diffractometer with Cu-Kα radiation (35 kV and 30 mA) at a scan rate of 1˚/min and was analyzed using standard software provided with the instrument. Thermogravimetric analysis and differential scanning calorimetry (TGA/DSC) were carried out using NETZSCH STA 409C. Thirty milligrams of the sample was used and alumina was used as reference. TGA and DSC curves were obtained from 25 to 650˚C at a rate of 10˚C/min.

2.5. Fluoride measurement

Fluoride was estimated by Orion ion selective electrode and Orion 720 A + ion analyzer. Total ionic strength adjusting buffer (TISAB—III) solution was added to both samples and standards in the ratio 1:10. TISAB—III contains 300 g $C_6H_5Na_3O_7{\cdot}2H_2O$, (FW = 294.10), 22 g of 1,2-Cyclohexanediamine-N,N,N′,N′-tetraaceticacid (CDTA), and 60 g of NaCl in a volume of 1,000 mL (pH: 5–5.5). TISAB—III solution regulates the ionic strength of samples and standard solutions, adjusts the pH, and also avoid interferences by polyvalent cations such as Al(III), Fe(III), and Si(IV), which are able to complex or precipitates with fluoride and reduces the free fluoride concentration in the solution. CDTA forms stable complexes with polyvalent metal cations (e.g. Al(III), Fe(III), and Si(IV)) which are more stable than metal-fluoride complexes ($AlF_6{}^{3-}$, $FeF_6{}^{3-}$, etc.) in solution. The CDTA preferentially complexes with polyvalent cations present in water and/or aqueous solution (e.g. Si^{4+}, Al^{3+}, and Fe^{3+}). Sodium citrate in TISAB—III is a complexing agent. It forms complexes with aluminum, iron, magnesium, silicates, etc. and reduces the interference due to aluminum, iron, magnesium, silicates, etc. The electrode is selective for the fluoride ion over other common anions by several orders of magnitude.

2.6. Batch experiments

The batch experiments to study the removal of fluoride from solution were carried out by treating 100 mL of fluoride solution in 250-mL conical flask with 0.4 g of the adsorbent. The conical flasks were immersed in a shaking water bath at predetermined temperatures (25, 35, and 45˚C). The shaker speed was controlled at 400 rpm. After a predetermined contact time, the aqueous samples in each bottle were decanted and centrifuged at 4,500 rpm for 5 min, and then filtered through a 0.45 μm cellulose acetate filter. The supernatant liquid was analyzed for total dissolved fluoride.

The effect of contact time (5 min – 8 h) was examined at 25 and 45˚C with initial fluoride concentration at 10 mg/L. Adsorption isotherm studies were conducted by varying initial fluoride concentrations (1, 5, 10, 15, 20, 25, 30, 35, 40, 45, and 50 mg/L) at different temperatures (i.e. 25, 35, and 45˚C). The effect of pH of the solution was investigated by adjusting the solution at different pH (2.2 to 9.5) using 0.05 M HCl and 0.05 M NaOH solutions with an initial fluoride concentration of 10 mg/L. To determine the effect of other competitive anions on fluoride adsorption, batch experiments were performed using solutions of 10 mg/L fluoride containing 20 to 160 mg/L of phosphate (PO_3^{3-}), bicarbonate (HCO_3^-), carbonate (CO_3^{2-}), sulfate (SO_4^{2-}), chloride (Cl^-), and nitrate (NO_3^-) separately. After a 1 h contact time at ambient temperature, the suspension was filtered through a 0.45 μm cellulose acetate filter and analyzed for total fluoride.

2.7. Desorption experiments

The reusability of used polyaniline/BOF slag nanocomposite samples mainly depends on the ease with which fluoride gets desorbed from loaded adsorbent samples. Desorption study was carried out by treating 100 mL NaF solution of 1, 5, and 10 mg/L with 0.4 g of polyaniline/BOF slag nanocomposite and was kept for a contact time of 24 h. The contents of the flask was filtered and separated. The exhausted adsorbent was retreated with 100 mL of distilled water maintained at pH 2–12 and was kept for a contact time of 24 h. The residual fluoride concentration was measured.

3. Result and discussion

3.1. Characterization of BOF slag and polyaniline/BOF slag nanocomposite

The principal chemical compositions of the BOF slag are shown in Table 1. The BOF slag consisted mainly of CaO, Fe_2O_3, SiO_2, Al_2O_3, FeO, and MgO (more than 90% by mass). It is evident from Table 2 that for ball-milled BOF slag, density, surface area, and total porosity increased. This could be regarded as effect of mechanochemistry while BOF slag was being ground. On the other hand, thermal activation leaded to show BOF slag more porous and bigger surface areas than thermally untreated BOF slag, while density of materials decreased. Percentage removal of fluoride (10 mg/L, 25℃, and 0.4 g/100 mL adsorbent dose) was higher for thermally activated BOF slag and hence thermally activated BOF slag was taken for the synthesis of polyaniline/BOF slag nanocomposite. The specific surface area, total porosity, and percentage fluoride removal of polyaniline/BOF slag nanocomposite was higher than that of treated (milled & thermally treated) BOF slag.

The SEM (Scanning Electron Microscopy) images of thermally treated BOF slag and polyaniline/BOF slag nanocomposite before and after adsorption of fluoride ions are shown in Fig. 1(a)–(c). Fig. 1(a) corresponds to thermally treated BOF slag. It is evident from the figure that by milling followed by thermal activation, more and more pores were exposed, and it was predicted that these pores would exhibit positive effect on adsorption. Milling and thermal activation leaded to an increase in porosity and volume. Fig. 1(b) corresponds to polyaniline/BOF slag nanocomposite before adsorption. In the image, polymers are seen as spongy-like structures and BOF slag as crystalline particles.

Fig. 1(c) shows SEM image of polyaniline/BOF slag nanocomposite after fluoride adsorption. Energy dispersive X-ray spectroscopy (EDS or EDX) of the bright spots on the crystalline particles were obtained. The result indicated the presence of fluoride ions on the surface of polyaniline/BOF slag nanocomposite. This may be due to the adsorption of fluoride ions on the surface of the nanocomposite. It is also evident from SEM micrographs that most of the particles were within the size of 25 nm (0.025 μm).

The XRD (X-ray Diffraction) studies of treated BOF slag, polyaniline/BOF slag nanocomposite, and fluoride-adsorbed polyaniline/BOF slag nanocomposite are shown in Fig. 2(a)–(c). Fig. 2(a) and (b) corresponds to treated BOF slag and polyaniline/BOF slag nanocomposite, respectively. Fig. 1(a) shows sharp peaks and hence the treated BOF slag was well crystalline in nature. It is evident from Fig. 2(a) and (b) that the major minor products were RO phase (R → Divalent metal & RO → Divalent metal oxides), calcium oxide, dicalcium silicate, and tricalcium silicate. Fig. 2(c) corresponds to fluoride-adsorbed polyaniline/BOF slag nanocomposite. Phases of calcium fluoride were found in addition to the phases of metal oxides. So, the formation of insoluble calcium fluoride may be considered as one of the mechanisms of fluoride removal.

Table 1
Chemical composition of original BOF slag

Chemical composition	Content (%)
Silica (as SiO_2)	13.8
Calcium (as CaO)	46.5
Iron (as Fe_2O_3 and FeO)	16.7
Magnesium (as MgO)	7.4
Alumina (as Al_2O_3)	6.6
H_2O at 105℃	1.2
H_2O at 950℃	2.3

The FTIR (Fourier transform infrared spectroscopy) spectra of the polyaniline/BOF slag nanocomposite before and after adsorption with fluoride ions are shown in Fig. 3. The FTIR spectrum of the polyaniline/BOF slag nanocomposite demonstrated six principal absorptions at 1,591, 1,506, 1,305, 1,211, 1,146, and 832 cm^{-1} [37]. The peaks at 1,591 and 1,506 cm^{-1} are assigned to C–C ring stretching vibrations. The peaks at 1,305 and 1,211 cm^{-1} correspond to N–H bending and the symmetric component of the C–C (or C–N) stretching modes. The bands at 1,146 and 832 cm^{-1} can be attributed to the in-plane and out-of-plane C–H bending modes, respectively [38]. The band characteristic of conducting form is observed at 1,211 cm^{-1} [39]. It has been interpreted as originating from bi-polaron structure, related to C–N stretching vibration. The peak at 1591 cm^{-1} confirms the presence of conducting imine function. The C–Cl stretching peak arises in the region 590−700 cm^{-1} [37]. These results confirm the presence of conducting polyaniline moieties in the polyaniline/BOF slag nanocomposite. The polyaniline component in the nanocomposite after adsorption showed peaks at 1,595, 1,512, 1,308, 1,245, 1,148 and 835 cm^{-1} [37]. The peaks at 1,595 and 1,512 cm^{-1} are assigned to C–C ring stretching vibrations. The peaks at 1,308 and 1,245 cm^{-1} correspond to N-H bending and the symmetric component of the C–C (or C–N) stretching modes. The bands at 1,148 and 835 cm^{-1} can be attributed to the in-plane and out-of-plane C–H bending modes, respectively [38]. It is interesting to note that all peak positions are shifted towards higher value in case of the polyaniline/BOF nanocomposites after adsorption with fluoride ions. It is well known that the skeletal vibration, which involves the delocalized π electrons, is affected by the doping ions of the polymer [40]. This indicates that the more electronegative fluoride ions are adsorbed on the surface of the polyaniline/BOF nanocomposites by replacing doped chloride ions.

The thermal stability of polyaniline/BOF slag nanocomposite in air was investigated using thermogravimetric analysis (TGA) and differential scanning calorimetry (DSC), as shown in Fig. 4. The DSC curve

Table 2
Physical properties of BOF slag and polyaniline/BOF slag nanocomposite

Physical properties	Original BOF slag	BOF slag treated by milling	Thermally activated BOF slag	Polyaniline/BOF slag composite
Density (mg/cm^3)	3.23	3.42	2.76	2.11
Specific surface (m^2/g)	5.62	16.75	40.89	73.82
Total porosity (%)	9.74	12.23	17.89	33.28
Fluoride removal of phosphate (10 mg/L) %	66	68	71	85

of the polyaniline/BOF slag nanocomposite reveled that the process was endothermic up to the temperature of 178.3℃ and then the process becomes exothermic after 178.3℃. The 5.8% weight loss (from TGA) around 178.3℃ may be attributed to the water content. The weight loss around 490℃ can be assigned to the thermal degradation and complete decomposition of polyaniline in the nanocomposite. The strong exothermic peaks around 490℃ were observed in the DSC curve due to thermal degradation and complete decomposition of polyaniline in the nanocomposite. The temperature ranges of the exothermic peaks in the DSC curve fit well with those of weight loss in the TGA curve.

3.2. Batch experiments

3.2.1. Effect of contact time

The fluoride adsorption kinetic study was carried out with adsorbent dosage of 4 g/L and initial fluoride concentration of 10 mg/L at 25 and 45℃, respectively. Results are shown in Fig. 5. The figure demonstrates that adsorbed fluoride significantly increased with an increase in contact time. The adsorption rate was rapid in the initial stage (5–10 min) and later on it gradually slowed down. The slower adsorption was likely due to the decrease in adsorption sites on the surface of the nanocomposite [41]. About 58% of fluoride was removed in 10 min at 45℃, while only 43% at 25℃. Fluoride concentration was relatively constant at contact times > 35 min. The kinetic data shows that fluoride removal mainly occurred within 35 min and there was no significant change in residual fluoride concentrations after this time up to 8 h. This suggests that equilibrium of fluoride adsorption was roughly attained within 35 min.

Results also reveal that the uptake rates of fluoride increased with increase in temperature. Other investigators also reported that the fluoride removal rate and the capacity of the adsorbents increased with increase in temperature [10–13].

3.2.2. Adsorption kinetics

An appropriate kinetic model is often used for quantifying the changes in adsorption with time. Pseudo-first-order equation was employed to analyze the kinetic data since it allows evaluating effective adsorption capacity and the rate constant of the kinetic model without any parameters beforehand [42,43]. The pseudo-first-order Lagergren equation is shown in Eq. (1).

$$\log(q_e - q) = \log q_e - K_1\left(\frac{t}{2.303}\right) \tag{1}$$

where q is the amount of fluoride adsorbed at time t (mg/g), q_e is the amount of fluoride adsorbed at equilibrium (mg/g), and K_1 is the equilibrium rate constant of pseudo-first-order adsorption.

The plot of $\log(q_e - q)$ vs. t (contact time) is shown in Fig. 6. The straight line plots of $\log(q_e - q)$ against t indicate the validity of Lagergren rate equation of first-order kinetics. K_1, q_e, and correlation coefficients R^2 values under different conditions were calculated from these plots and are given in Table 3. High correlation coefficients ($R^2 > 0.99$) were observed for all fits, which indicates that the adsorption reaction could be approximated with a pseudo-first-order kinetic model. It suggests that the overall rate of the fluoride adsorption process should be controlled by the chemical process in accordance with the pseudo-first-order reaction mechanism.

3.2.3. Webber and Morris model

The use of the intraparticle diffusion model has been greatly explored to analyze nature of the rate-controlling step, which is represented by Eq. (2) [44].

$$q = K_p t^{1/2} \tag{2}$$

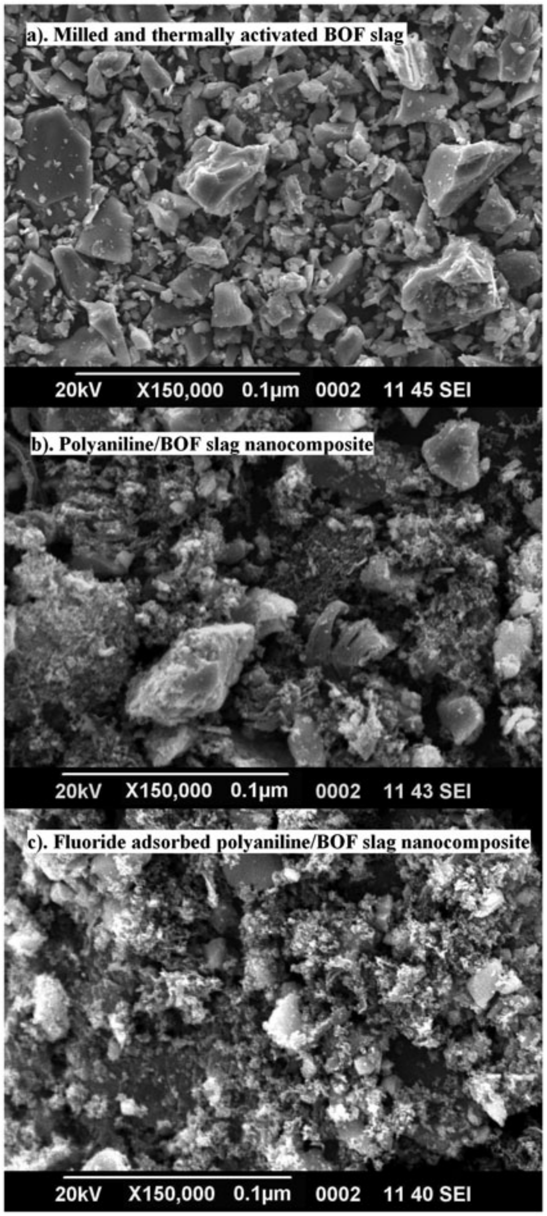

Fig. 1. SEM micrographs (magnification 150,000×).

where “K_p” is intraparticle diffusion rate constant and “t” is the contact time. According to this model, if the adsorption of solute is controlled by the intraparticle diffusion process, a plot of solute adsorbed against square root of contact time should yield a straight line passing through origin. The Weber and Morris plot of fluoride adsorption on polyaniline/BOF slag nanocomposite is shown in Fig. 7. It is evident from the figure that the plot of solute adsorbed against square root of contact time was a straight line, but not passing through origin. Straight lines with correlation coefficients (R^2) > 0.98 indicate that, the initial phase of the removal process may be controlled by the intraparticle diffusion. The greater diffusion rate in the early stage is attributed to higher fluoride concentration and available vacant sites at interior surfaces. Afterwards, the intraparticle diffusion began to slow down due to the low fluoride concentration in solution [42]. The diffusion resistance also increased with the increase in the interior adsorption, which led to a decrease in diffusion rate [43]. The intraparticle diffusion rate was obtained from the slope of the steep-sloped portion (Initial 30 min) (Table 3). The diffusion rate for fluoride at 25˚C was greater than that at 45˚C, indicating that fluoride was more easily diffused and transported into adsorbent pores at low temperature.

3.2.4. Effect of initial fluoride concentration and adsorption isotherms

Effect of initial fluoride concentration on fluoride adsorption was investigated at initial fluoride concentrations between 1 and 50 mg/L at 25, 35, and 45˚C. The fluoride loadings on the adsorbent (q_e) were calculated from the equilibrium fluoride concentrations (C_e). The adsorption loadings varied in the ranges of 0.79–9.12, 0.88–9.43, and 0.97–9.98 mg/g at 25, 35, and 45˚C, respectively. It indicates that fluoride adsorption increased with the increase in temperature. The adsorption isotherm data (q_e vs. C_e) were fitted to Langmuir and Freundlich adsorption isotherm models (Eqs. (3) and (4), respectively). Langmuir isotherm model assumes a monolayer surface coverage limiting the adsorption due to the surface saturation [3,44], while Freundlich isotherm model is an empirical model allowing for multilayer adsorption [9].

$$\frac{1}{q_e} = \frac{1}{q_0 b C_e} + \frac{1}{q_0} \tag{3}$$

$$\log q_e = \log K_f + n \log C_e \tag{4}$$

where C_e is the equilibrium fluoride concentration in the solution (mg/L), q_e is the amount adsorbed on the adsorbent at equilibrium (mg/g), q_0 is the maximum adsorption capacity (mg/g), b is a constant related to the adsorption energy (L/mg), K_f is the Freundlich constant denoting the adsorption capacity of the adsorbent [(mg/g)(L/mg)^n], and n is the adsorption intensity parameter. Values of $0.1 < n < 1$ show favorable adsorption of fluoride onto adsorbents.

All the adsorption data obtained were fitted to both the models as shown in Fig. 8(a) and (b). It was observed that the correlation coefficients for Langmuir

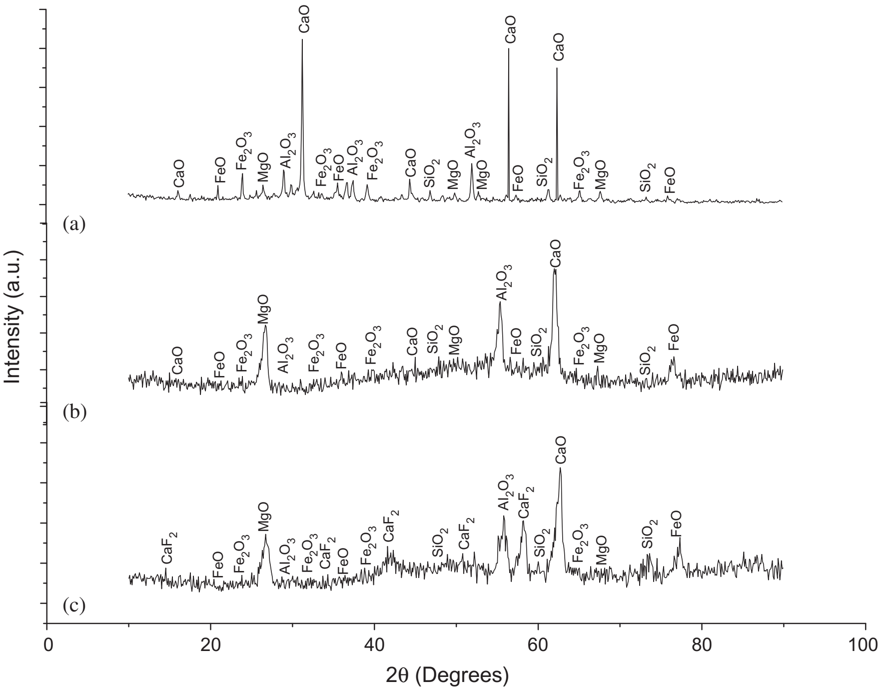

Fig. 2. XRD pattern of (a) milled and thermally activated BOF slag, (b) polyaniline/BOF slag nanocomposite and (c) fluoride-adsorbed polyaniline/BOF slag nanocomposite.

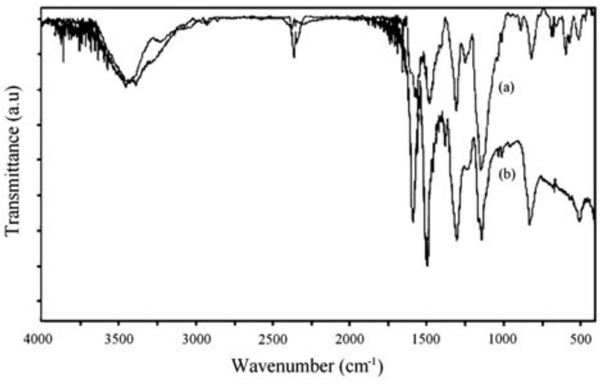

Fig. 3. FTIR spectrum of (a) polyaniline/BOF slag nanocomposite and (b) fluoride-adsorbed polyaniline/BOF slag nanocomposite.

isotherm model ($R^2 = 0.99$) were a little higher compared to those for Freundlich ($R^2 = 0.98$) (Table 4). Therefore, Langmuir isotherm yielded better fit to the experimental data with regard to fluoride adsorption on polyaniline/BOF slag nanocomposite at temperatures of 25, 35, and 45˚C. These facts suggest that fluoride was adsorbed in the form of monolayer coverage on the surface of the adsorbent.

The values of maximum adsorption capacity (q_0) and Langmuir constant (b) were evaluated from the intercept and slope of the Langmuir plots, and are given in Table 4. Results show the maximum amount of fluoride was removed at 45˚C, followed by, at 35, and 25˚C. It demonstrates that adsorption capacity increased with an increase in reaction temperature. The values of K_f and n were obtained from the slope and intercept of the linear Freundlich plots and listed in Table 4. The K_f indicating the adsorption capacity of the adsorbent increased with an increase in reaction temperature, which is consistent with the

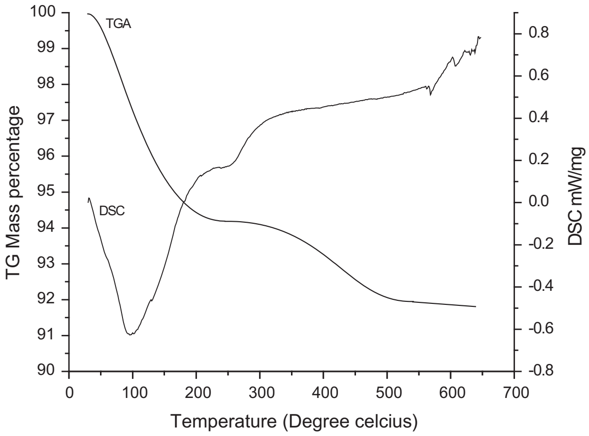

Fig. 4. Thermogravimetric analysis and differential scanning calorimetry of polyaniline/BOG slag nanocomposite up to 650˚C.

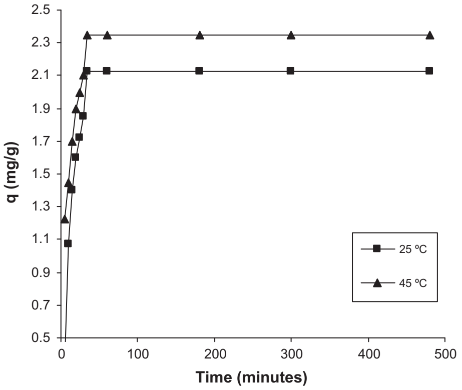

Fig. 5. Effect of contact time on fluoride adsorption on polyaniline/BOF slag nanocomposite (initial fluoride concentration = 10 mg/L and adsorbent dosage = 4 g/L).

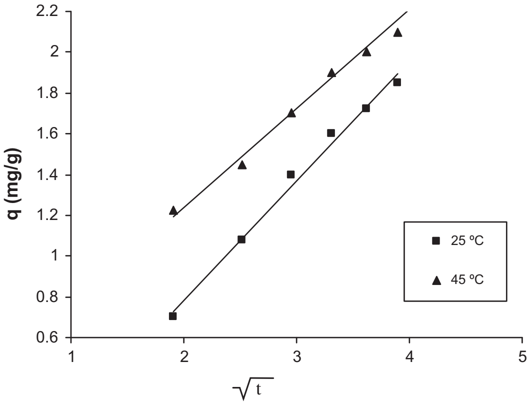

Fig. 7. Plot of Webber and Morris diffusion rate equation for fluoride adsorption on polyaniline/BOF slag nanocomposite at 25 and 45˚C.

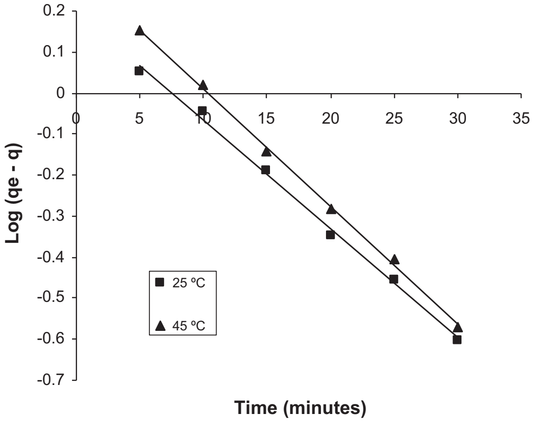

Fig. 6. Plot of Lagergren's pseudo-first-order rate equation for fluoride adsorption on polyaniline/BOF slag nanocomposite at 25 and 45˚C.

results of Langmuir model. The calculated *n* lies in the range between 0.32 and 0.37, denoting favorable adsorption of fluoride onto polyaniline/BOF slag nanocomposite.

It is known that the Langmuir and Freundlich adsorption isotherm constant do not give any idea about the adsorption mechanism. In order to understand the adsorption type, equilibrium data were tested with Dubinin—Radushkevich isotherm. The linearized D.R. equation is represented by Eq. (5) [3,9,44];

$$\ln q_e = \ln q_m - K\varepsilon^2 \tag{5}$$

where ε is polanyi potential, and is equal to $RT \ln(1 + 1/C_e)$, q_e is the amount of fluoride adsorbed per unit mass of adsorbent, q_m is the theoretical adsorption capacity, C_e is the equilibrium concentration of fluoride, K is the constant related to adsorption energy, R is universal gas constant, and T is the temperature in Kelvin. Fig. 8(c) shows the plot of $\ln q_e$ against ε^2, which was almost linear with correlation coefficients, $R^2 = 0.978$. D.R. isotherm constants K and q_m were calculated from the slope and intercept of the plot, respectively. The values of K were found to be 2.185×10^{-3}, 2.035×10^{-3}, and 1.958×10^{-3} mol^2 kJ^{-2} and those of q_m were 5.512, 5.624, and 5.765 mg/g at 25, 35, and 45˚C, respectively. The mean free energy of adsorption (E) was calculated from the constant K using Eq. (6) [3,9,44].

Table 3
Rate constants (K_1) obtained from Lagergren rate equation and intraparticle diffusion rate constants obtained from Weber—Morris equation for adsorption of fluoride on polyaniline/BOF slag nanocomposite at different temperatures

	Lagergren rate equation				Weber—Morris equation			
Temperature	Slope	Intercept	Rate constant in min^{-1} (K_1)	R^2	Slope	Intercept	Rate of pore diffusion (k_p)	R^2
25˚C	−0.0226	0.201	0.061	0.996	0.585	−0.384	0.585	0.991
45˚C	−0.0286	0.296	0.065	0.998	0.484	0.269	0.484	0.986

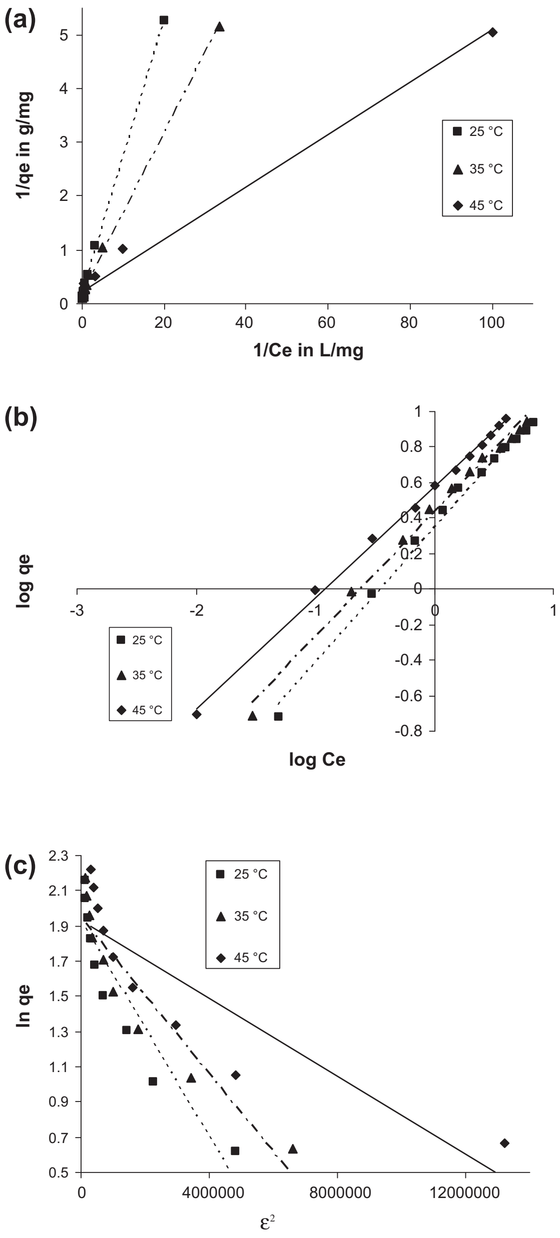

Fig. 8. Langmuir, Freundlich, and DR adsorption isotherms for fluoride adsorption on polyaniline/BOF slag nanocomposite.

$$E = (2K)^{-1/2} \tag{6}$$

E is defined as the free energy change when 1 mol of ion is transferred to the surface of the solid from infinity in solution. The values of E were found to be 15.127, 15.674, and 15.980 kJmol^{-1} at 25, 35, and 45℃ respectively. The value of E is very useful in predicting the type of adsorption. If the value of E is less than 8 kJmol^{-1}, then the adsorption is physical in nature and if it is in between 8–16 kJmol^{-1}, then the adsorption is due to exchange of ions [3,9,44]. The values found in the present study were in between 8–16 kJmol^{-1}. So, the adsorption can be best explained as ion exchange process.

3.2.5. Thermodynamic study

To evaluate the thermodynamic feasibility and to confirm the nature of the adsorption process, three basic thermodynamic parameters, standard free energy (ΔG°), standard enthalpy (ΔH°), and standard entropy (ΔS°) were calculated using the following equations (Eqs. (7)–(9)).

$$\Delta G^\circ = -RT \ln\left(\frac{1}{b}\right) \tag{7}$$

$$\ln b = \ln b_0 - \frac{\Delta H^\circ}{RT} \tag{8}$$

$$\Delta G^\circ = \Delta H^\circ - T\Delta S^\circ \tag{9}$$

where b is Langmuir constant which is related to the energy of adsorption, b_0 is a constant, R is the universal gas constant (8.314 J/(mol K)), and T is the temperature in Kelvin (K). Calculated values of the thermodynamic parameters ΔG°, ΔH°, and ΔS° are given Table 5. The negative ΔG° values indicate the adsorption process was spontaneous. The value of ΔH° for fluoride adsorption was 33.164 kJ/mol, suggesting that the interaction between fluoride and polyaniline/BOF slag nanocomposite was endothermic in nature. Hence, it can be concluded that the nature of fluoride adsorption was chemical (ion exchange), which is in accordance with the results of kinetic study. The decrease in ΔG° with the rise in temperature shows an increase in feasibility of adsorption at higher temperatures. The positive ΔS° values indicate some structural changes in adsorbate and adsorbent during adsorption reaction.

3.2.6. Effect of pH

pH is an important parameter which influences most of the solid/liquid adsorption processes. Fluoride adsorption behavior of polyaniline/BOF slag nanocomposite was explored under different pH conditions to understand the fluoride removal mechanism and to determine the pH region of maximum performance of the nanomaterial. Results are shown in Fig. 9. It is evident from the figure that the percentage removal of fluoride by polyaniline/

Table 4
Langmuir and Freundlich constants for fluoride adsorption on polyaniline/BOF slag nanocomposite at different temperatures

	Langmuir constants			Freundlich constants		
Temperature	q_0 (mg/g)	b (L/mg)	R^2	n	K_f (mg/g)(L/mg)^n	R^2
25℃	5.438	0.742	0.997	0.370	0.148	0.985
35℃	7.532	0.645	0.998	0.368	0.225	0.983
45℃	9.143	0.318	0.996	0.325	0.367	0.982

BOF slag nanocomposite increased sharply from 21 to 86%, for an increase in equilibrium pH from 2.2 to 7.1 and then there was a slight decrease in the percentage removal, from 86 to 78%, with increase in pH from 7.1 to 9.5. Such a trend has been reported for several sorbent–fluoride sorption systems [45,46]. In the low pH region, the low fluoride uptake is due to the reduced availability of CaO (in polyaniline/BOF slag nanocomposite), which is one of the major constituent responsible for the removal of fluoride, while the slight reduction at high pH may result from competitive interaction with hydroxyl ions and electrostatic repulsion between some deprotonated active sites and fluoride. This is also attributed to the fact that a higher pH value causes the surface to carry more negative charges and thus would more significantly repel the negatively charged species in solution. Therefore, the slight decrease in adsorption of fluoride at higher pH values resulted from an increased repulsion between the more negatively charged F^- species and negatively charged surface sites. The values of zeta potential of polyaniline/BOF slag nanocomposite were measured and results are given in Fig. 10. The measured zeta potential shows the variation of surface charge from + 14.7 to −33.1 and + 16.1 to −31.5 mV, corresponding to a pH change from 2 to 12, at 0.01 M and 0.001 M NaCl solution, respectively. The point of zero charge (pH_{pzc}) value of polyaniline/BOF slag nanocomposite was found to be 7.1.

Table 5
Thermodynamic parameters for fluoride adsorption on polyaniline/BOF slag nanocomposite at different temperatures

Temperature	ΔG° (kJ/mol)	ΔH° (kJ/mol)	ΔS° (J/(mol K))
25℃	−0.740	33.164	113.772
35℃	−1.124		111.325
45℃	−3.033		113.826

Overall, results suggest that the nanocomposite is more effective in the near neutral and alkaline pH range. The pH of drinking water normally ranges from 6.5 to 8.5 and hence the nanocomposite is expected to perform optimally in drinking water defluoridation. For wastewater, pH adjustment may be required for optimal performance.

3.2.7. Effect of competitive ions

Drinking water and wastewater contains many competitive anions. Therefore, it was thought worthwhile to study the effect of competitive ions like phosphate, bicarbonate, carbonate, sulfate, chloride, and nitrate on the adsorption of fluoride. Varying concentration of these solutions was prepared from their sodium/potassium salts. The initial concentration of fluoride was fixed at 10 mg/L, while the initial concentration of other anions varied from 20 to 160 mg/L. The result of the study is given in Fig. 11. It is clear from the figure that the presence of these anions

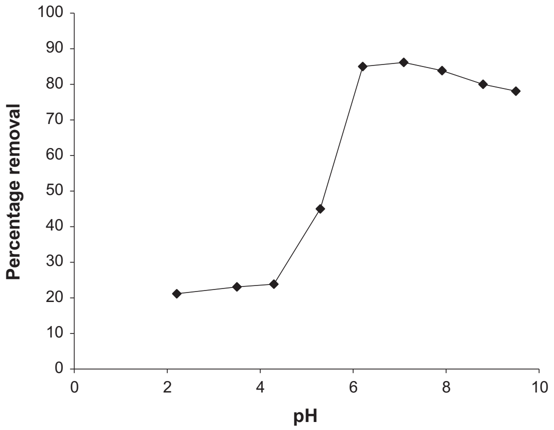

Fig. 9. Effect of equilibrium pH on fluoride adsorption onto polyaniline/BOF slag nanocomposite (initial fluoride concentration = 10 mg/L, temperature = 25℃, contact time = 35 min, and adsorbent dosage = 4 g/L).

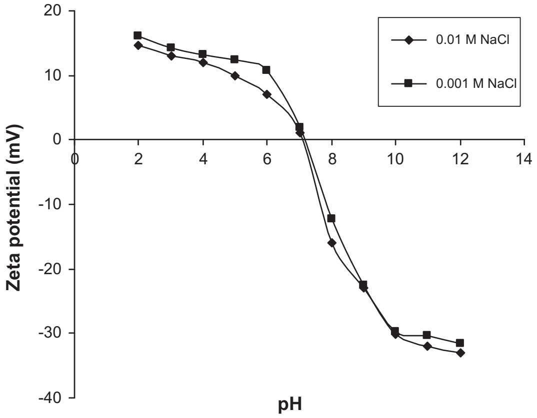

Fig. 10. Zeta potential of polyaniline/BOF slag nanocomposite as a function of pH using 0.01 M NaCl and 0.001 M NaCl as supporting electrolyte.

reduced the adsorption of fluoride appreciably. It is evident from the figure that the percentage removal of fluoride decreased gradually with increase in concentration of these anions. The anions reduced the fluoride adsorption in the order, phosphate > bicarbonate > carbonate > sulfate > chloride > nitrate. These results were in well agreement with those reported in literatures [47].

3.2.8. Desorption study

The result of the study is presented in Table 6. Desorption of the adsorbed fluoride at different pH was less than 4% for initial concentration of 1 mg/L, 5 mg/L, and 10 mg/L. It is evident from the low desorption values that the adsorption of fluoride onto polyaniline/BOF slag nanocomposite was chemical in nature. Chemisorption exhibits poor desorption, it may be due to the fact that in chemisorption the adsorbate species are held firmly to the adsorbent with comparatively stronger bonds. It is also evident from the table that there was slight decrease in percentage desorption with increase in pH. This may be due to the fact that, in acidic medium, CaF_2 so formed reacts with the acid to form calcium salt of the acid and liberate HF resulting in fluoride desorption.

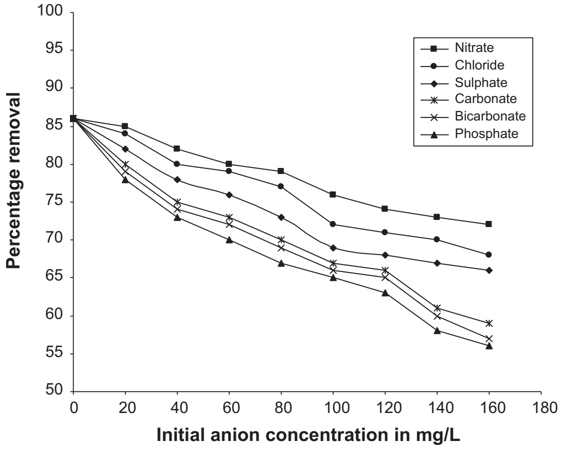

Fig. 11. Effect of presence of anions on fluoride adsorption (initial fluoride concentration = 10 mg/L, temperature = 25˚C, contact time = 35 min, and adsorbent dosage = 4 g/L).

3.3. Mechanism of fluoride removal

The mechanism of fluoride ion removal by the nanocomposite involves the interaction of fluoride ions with both the polyaniline and BOF slag moieties. It is well established that the removal of fluoride ions by BOF slag occurs due to the precipitation reaction, due to the formation of calcium fluoride. When the nanocomposite is added to water, CaO present is converted into calcium hydroxide. A part of which goes into the solution and the remaining is left as solid. The portion which goes into solution reacts with F^- to form CaF_2, which is insoluble and is left as precipitate. The major portion of calcium hydroxide does not go into solution. So, there is removal of fluoride by surface chemical reaction or ion exchange, in which hydroxide ions of calcium hydroxide are replaced by fluoride ions with the formation of CaF_2. Both of the above process can be represented by the following reaction (Eq. (10)).

$$Ca(OH)_2 + 2F^- \rightarrow CaF_2(s) + 2OH^- \tag{10}$$

This was further confirmed by the XRD analysis of polyaniline/BOF slag nanocomposite, before and after

Table 6
Percentage desorption of fluoride at pH (pH of 2, 4, 6, 8, 10, and 12) by polyaniline/BOF slag nanocomposite

	Percentage desorption					
Initial concentration	pH 2	pH 4	pH 6	pH 8	pH 10	pH 12
1 mg/L	3.646	3.444	3.242	2.933	2.635	2.424
5 mg/L	3.732	3.661	3.448	3.344	3.181	2.997
10 mg/L	3.798	3.755	3.722	3.615	3.346	3.117

the adsorption process (Fig. 2). The polyaniline/BOF slag nanocomposite, before adsorption, mainly contained the phases of calcium oxide. But the material retrieved after adsorption contained phases of calcium fluoride.

In the case of polyaniline which is employed in the form of chloride ion-doped polymer, fluoride ions were removed from aqueous solution through the replacement of doped ionisable chloride ions present in it, i.e. by ion exchange mechanism [34] as represented by Eq. (11). Therefore, in the present study, removal of fluoride ions by the polyaniline/BOF slag nanocomposite is a combination of mechanisms followed by constituents present in it.

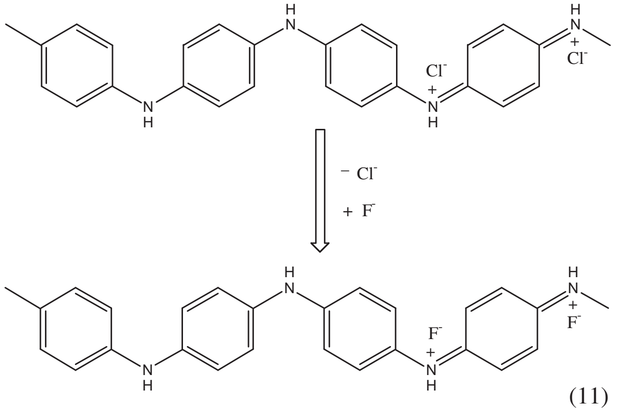

(11)

4. Conclusion

The present research investigated the evaluation of fluoride removal efficiency by polyaniline/BOF slag nanocomposite. BOF slag consisted mainly of CaO, Fe_2O_3, SiO_2, Al_2O_3, FeO, and MgO (more than 90% by mass). Fluoride removal efficiency was evaluated by studying the effect of various parameters. Fluoride adsorption onto polyaniline/BOF slag nanocomposite significantly increased with an increase in contact time. The adsorption rate was fast at the initial stage, followed by a slower rate, which well fitted the Lagergren first-order kinetic model. Equilibrium was established within 35 min. Temperature played an important role in the fluoride adsorption kinetics. At higher temperature, fluoride exhibited greater removal rates. The adsorption closely followed Langmuir adsorption isotherm at different temperatures. Thermodynamic study indicated that fluoride adsorption onto polyaniline/BOF slag nanocomposite was an endothermic process. The adsorption was spontaneous and favorable at the temperatures investigated. Fluoride removal was greatly affected by the initial pH of the solution. The fluoride adsorption was impeded by the presence of phosphate, followed by bicarbonate, carbonate, sulfate, chloride, and nitrate. The fluoride removal was probably due to chemisorption, precipitation, and surface chemical reaction with CaO present in the BOF slag and through the replacement of doped ionisable chloride ions present in polyaniline.

Acknowledgment

This project was supported by King Saud University, Deanship of Scientific Research, College of Science Research Center.

References

[1] WHO, Chemical fact sheets: fluoride, in: Guidelines for Drinking Water Quality (electronic resource): Incorporation First Addendum, 3rd ed., Recommendations, Geneva, 2006.
[2] M. Mohapatra, S. Anand, B.K. Mishra, D.E. Giles, P. Singh, Review of fluoride removal from drinking water, J. Environ. Manag. 91 (2009) 67–77.
[3] M. Islam, R.K. Patel, Evaluation of removal efficiency of fluoride from aqueous solution using quick lime, J. Hazard. Mater. 143 (2007) 303–310.
[4] T. Tsutsui, N. Suzuki, M. Ohmori, H. Maizumi, Cytotoxicity, chromosome aberrations and unscheduled DNA synthesis in cultured human diploid fibroblasts induced by sodium fluoride, Mutat. Res. 139 (1984) 193–198.
[5] M.A. Elrashidi, W.L. Lindsay, Solubility of aluminum fluoride, fluorite and fluoriphogopite minerals in soils, J. Soil Sci. Soc. Am. 50 (1986) 594–598.
[6] M. Bishnoi, A. Shalu, Potable groundwater quality in some villages of Haryana, India: Focus on fluoride, J. Environ. Biol. 28 (2007) 291–294.
[7] K. Shailaja, M.E.C. Johnson, Fluorides in groundwater and its impact on health, J. Environ. Biol. 28 (2007) 331–332.
[8] E. Oguz, Equilibrium isotherms and kinetics studies for the sorption of fluoride on lightweight concrete materials, Colloids Surf. A: Physicochem. Eng. Aspects 295 (2007) 258–263.
[9] M. Islam, P.C. Mishra, R.K. Patel, Fluoride adsorption from aqueous solution by a hybrid thorium phosphate composite, Chem. Eng. J. 166 (2011) 978–985.
[10] K.M. Popat, P.S. Anand, B.D. Dasare, Selective removal of fluoride ions from water by the aluminum form of the aminomethylphosphonic acid-type ion exchanger, React. Polym. 23 (1994) 23–32.
[11] H. Kodama, N. Kabay, Reactivity of inorganic anion exchanger $BiPbO_2(NO_3)$ with fluoride ions in solution, Solid State Ionics 141 (2001) 603–607.
[12] C.L. Yang, R. Dluhy, Electrochemical generation of aluminum sorbent for fluoride adsorption, J. Hazard. Mater. B 94 (2002) 239–252.
[13] Y. Zhou, C. Yu, Y. Shan, Adsorption of fluoride from aqueous solution on La^{3+} impregnated crosslinked gelatin, Sep. Purif. Technol. 36 (2004) 89–94.

[14] B.E. Smith, Desalting and groundwater management in the San Joaquin valley, Desalination 87 (1992) 151–174.

[15] S. Bouguecha, M. Dhahbi, The role of membrane technologies in supplying drinking and industrial water in Tunisia: Conventional process and new trends, Desalination 151 (2002) 75–86.

[16] K. Hu, J.M. Dickson, Nanofiltration membrane performance on fluoride removal from water, J. Membr. Sci. 279 (2006) 528–529.

[17] E. Kir, E. Alkan, Fluoride removal by Donnan dialysis with plasmamodified and unmodified anion-exchange membranes, Desalination 197 (2006) 217–224.

[18] Z. Amor, B. Bariou, N. Mameri, M. Taky, S. Nicolas, A. Elmidaoui, Fluoride removal from Corn brackish water by electrodialysis, Desalination 133 (2001) 215–223.

[19] M. Tahaikt, I. Achary, M.A. Menkouchi Sahli, Z. Amor, M. Taky, A. Alami, A. Boughriba, M. Hafsi, A. Elmidaoui, Defluoridation of Moroccan ground water by electrodialysis: continuous operation, Desalination 167 (2004) 357–365.

[20] G. Jiantuan, Q. Jiuhui, L. Pengju, L. Huijuan, New bipolar electrocoagulation–electroflotation process for the treatment of laundry wastewater, Sep. Purif. Technol. 36 (2004) 33–39.

[21] M. Liu, R.Y. Sun, J.H. Zhang, Y. Bina, L. Wei, P. Lui, F. Keichero, Elimination of excess fluoride in potable water with coarcervation by electrolysis using aluminum anode, Fluoride 20 (1983) 54–63.

[22] T.C. Chuang, C.J. Huang, J.C. Liu, Treatment of semiconductor wastewater by dissolved air flotation, J. Environ. Eng. 128 (2002) 974–980.

[23] F. Shen, X. Chen, P. Gao, G. Chen, Electrochemical removal of fluoride ions from industrial wastewater, Chem. Eng. Sci. 58 (2003) 987–993.

[24] B. Kemer, D. Ozdes, A. Gundogdu, V.N. Buluta, C. Duran, M. Soylak, Removal of fluoride ions from aqueous solution by waste mud, J. Hazard. Mater. 168 (2009) 888–894.

[25] S. Kumar, A. Gupta, J.P. Yadav, Fluoride removal by mixtures of activated carbon prepared from Neem (*Azadirachta indica*) and Kikar (*Acacia arabica*) leaves, Ind. J. Chem. Tech. 14 (2007) 355–361.

[26] A.J. Arulanantham, T.V. Ramakrishna, N. Balasubramanium, Studies on fluoride removal by coconut shell carbon, Ind. J. Environ. Health. 12 (1992) 531–536.

[27] R. Sivabalan, S. Rengaraj, B. Arabindoo, V. Murugesan, Fluoride uptake characteristics of activated carbon from agriculture-waste, J. Sci. Ind. Res. 61 (2002) 1039–1045.

[28] Y.H. Li, S. Wang, A. Cao, D. Zhao, X. Zhang, C. Xu, Z. Luan, D. Ruan, J. Liang, D. Wu, B. Wie, Adsorption of fluoride from water by amorphous alumina supported on carbon nanotubes, Chem. Phys. Let. 322 (2001) 1–5.

[29] D.J. Killedar, D.S. Bhargava, Effects of stirring rate and temperature on fluoride removal by fishbone charcoal, Ind. J. Environ. Health. 35 (1993) 81–87.

[30] S. Meenakshi, N. Viswanathan, Identification of selective ion-exchange resin for fluoride sorption, J. Colloid Interface Sci. 308 (2007) 438–450.

[31] P.K. Shrivastava, A. Deshmukh, Defluoridation of water with natural zeolite, J. Ind. Phys. Health Environ. 4 (1994) 11–14.

[32] S.S. Tripathy, A.M. Raichura, Abatement of fluoride from water using manganese dioxide-coated activated alumina, J. Hazard. Mater. 153 (2008) 1043–1051.

[33] O.J. Hao, C.P. Huang, Adsorption characteristics of fluoride onto hydrous alumina, J. Environ. Eng. 112 (1986) 1054–1069.

[34] M. Karthikeyan, K.K. Satheeshkumar, K.P. Elango, Removal of fluoride ions from aqueous solution by conducting polypyrrole, J. Hazard. Mater. 167 (2009) 300–305.

[35] K. Laszlo, P. Podkoscielny, A. Dabrowski, Heterogeneity of activated carbons with different surface chemistry in adsorption of phenol from aqueous solutions, Appl. Surf. Sci 252 (2006) 5752–5762.

[36] M.G. Sujana, R.S. Thakur, S.B. Rao, Removal of fluoride from aqueous solution by using alum sludge, J. Colloid Interface Sci. 206 (1998) 94–101.

[37] P.S. Rao, J. Anand, S. Palaniappan, D.N. Sathyanarayana, Effect of sulphuric acid on the properties of polyaniline-HCl salt and its base, Eur. Polym. J. 36 (2000) 915–921.

[38] A. Maity, S. Sinha Ray, Highly conductive core–shell nanocomposite of poly N-vinylcarbazole–polypyrrole with multi wall carbon nanotubes, Macromol. Rapid Commun. 29 (2008) 1582–1587.

[39] A.M.P. Hussain, A. Kumar, Electrochemical synthesis and characterization of chloride doped polyaniline, Bull. Mater. Sci. 26 (2003) 329–334.

[40] M.R. Karim, C.J. Lee, A.M.S. Chowdhury, N. Nahar, M.S. Lee, Radiolytic synthesis of conducting polypyrrole/carbon nanotube composites, Mater. Lett. 61 (2007) 1688–1692.

[41] S. Goldberg, Competitive adsorption of arsenate and arsenite on oxides and clay minerals, Soil Sci. Soc. Am. J. 66 (2002) 413–421.

[42] M. Badruzzaman, P. Westerhoff, D.R.U. Knappe, Intraparticle diffusion and adsorption of arsenate onto granular ferric hydroxide (GFH), Water Res. 38 (2004) 4002–4012.

[43] Y. Kim, C. Kim, I. Choi, S. Rengaraj, J. Yi, Arsenic removal using mesoporous alumina prepared via a templating method, Environ. Sci. Technol. 38 (2004) 924–931.

[44] M. Islam, R.K. Patel, Synthesis & physicochemical characterization of Zn/Al chloride layered double hydroxide and evaluation of its nitrate removal efficiency, Desalination 256 (2010) 120–128.

[45] A. Eskandarpour, M.S. Onyango, A. Ochieng, S. Asai, Removal of fluoride ions from aqueous solution at low pH using schwertmannite, J. Hazard. Mater. 152 (2008) 571–579.

[46] S. Kagne, S. Jagtap, P. Dhawade, S.P. Kamble, S. Devotta, S.S. Rayalu, Hydrated cement: A promising adsorbent for the removal of fluoride from aqueous solution, J. Hazard. Mater. 154 (2008) 88–95.

[47] M. Mahramanlioglu, I. Kizilcikli, I.O. Bicer, Adsorption of fluoride from aqueous solution by acid treated spent bleaching earth, J. Fluorine Chem. 115 (2002) 41–47.